

Co-location of the downdip end of seismic coupling and the continental shelf break

Luca C. Malatesta^{1,2,3}, Lucile Bruhat⁴, Noah J. Finnegan¹, Jean-Arthur L.
Olive⁴

¹Department of Earth and Planetary Sciences, University of California Santa Cruz, Santa Cruz,
California, USA.

²Institute of Earth Surface Dynamics, University of Lausanne, Lausanne, Switzerland

³Earth Surface Process Modelling, GFZ German Research Center for Geosciences, Potsdam, Germany

⁴Laboratoire de Géologie, UMR 8538, École Normale Supérieure, PSL University, CNRS, Paris, France

Key Points:

- Shelf breaks at subduction margins lie above the downdip end of seismic coupling.
- Spatial patterns of interseismic deformation are reflected in long-term subduction margin uplift.
- The morphology of a subduction margin integrates deformation from hundreds of seismic cycles.

Corresponding author: Luca C. Malatesta, luca.malatesta@gfz-potsdam.de

Abstract

16
17 Along subduction margins, the morphology of the near shore domain records the com-
18 bined action of erosion from ocean waves and permanent tectonic deformation from the
19 convergence of plates. We observe that at subduction margins around the globe, the edge
20 of continental shelves tends to be located above the downdip end of seismic coupling on
21 the megathrust. Coastlines lie farther landward at variable distances. This observation
22 stems from a compilation of well-resolved coseismic and interseismic coupling datasets.
23 The permanent interseismic uplift component of the total tectonic deformation can ex-
24 plain the localization of the shelf break. It contributes a short wave-length gradient in
25 vertical deformation on top of the structural and isostatic deformation of the margin.
26 This places a hinge line between seaward subsidence and landward uplift above the downdip
27 end of high coupling. Landward of the hinge line, rocks are uplifted in the domain of wave-
28 base erosion and a shelf is maintained by the competition of rock uplift and wave ero-
29 sion. Wave erosion then sets the coastline back from the tectonically meaningful shelf
30 break. We combine a wave erosion model with an elastic deformation model to illustrate
31 how the downdip end of high coupling pins the location of the shelf break. In areas where
32 the shelf is wide, onshore geodetic constraints on seismic coupling is limited and could
33 be advantageously complemented by considering the location of the shelf break. Sub-
34 duction margin morphology integrates hundreds of seismic cycles and could inform seis-
35 mic coupling stability through time.

1 Introduction

36
37 The area of a subduction interface that is frictionally coupled between earthquakes
38 controls the size of megathrust ruptures (Aki, 1967; Mai & Beroza, 2000). Strain accu-
39 mulation from partial coupling of the plate interface (Wang & Dixon, 2004; Lay & Schwartz,
40 2004) produces interseismic deformation at the surface, which can be inverted to deter-
41 mine the extent of the fully, or strongly, coupled region on the fault, following the widely
42 used back slip model (Savage, 1983). This procedure has been used for decades to pro-
43 duce maps of coupling over subduction zones (e.g. Yoshioka et al., 1993; Sagiya, 1999;
44 Mazzotti et al., 2000; Nishimura et al., 2004; Simoes et al., 2004; Chlieh et al., 2008; Metois
45 et al., 2012). However, due to the short duration of geodetic measurements, these inver-
46 sions typically reflect a fraction of the earthquake cycle, which could be contaminated
47 by transient slip events (Dragert et al., 2001; Obara, 2002), postseismic deformation from

48 previous large earthquakes (e.g. Trubienko et al., 2013; Sun et al., 2018), or deforma-
49 tion unrelated to the megathrust (such as postglacial rebound, James et al., 2009). Be-
50 cause the coupled region is typically offshore, it may also be poorly constrained simply
51 due to the concentration of geodetic measurements on land. This problem is compounded
52 by wide continental shelves (Wang & Tréhu, 2016). Seafloor geodesy can overcome some
53 of these problems, but remains uncommon (Bürgmann & Chadwell, 2014). Any progress
54 toward better constraining the size of coupled patches is an important goal for the seis-
55 motectonic community.

56 On land, tectonic geomorphology complements short duration geodetic and seis-
57 mic records and provides a meaningful tectonic record that is often missing offshore (e.g.
58 Valensise & Ward, 1991; Lavé & Avouac, 2001; Brooks et al., 2011). During the seismic
59 cycle, crustal deformation is considered as almost entirely elastic and balanced by co-
60 seismic deformation. But over geological time scales, herein *long-term* ($> 10^5$ yrs), the
61 small fraction of deformation that is anelastic and permanent would accumulate and shape
62 the morphology of the margin (Bilham et al., 1997; Avouac, 2003). Meade (2010) for ex-
63 ample identified a first-order similarity between interseismic deformation and permanent
64 uplift by comparing an interseismic deformation model to the pattern of fluvial erosion
65 across the Himalayas.

66 Among the little work that has linked submarine geomorphology and subduction
67 zone deformation, Ruff and Tichelaar (1996) identified a correlation between the downdip
68 end of subduction zone rupture and the position of the coastline. This correlation fits
69 the Andean subduction particularly well, and Saillard et al. (2017) suggested that the
70 distribution of anelastic interseismic deformation could explain it. However, the posi-
71 tion of the coastline at active margins depends on several processes that are not tectonic
72 in nature, the most important of which is the ever-varying sea level. The current loca-
73 tion of the coastline is specific to the present sea level high-stand; at the last glacial max-
74 imum, ~ 20 ka, global sea level was at a low-stand that was on average ~ 125 m lower than
75 present level (Spratt & Lisiecki, 2016). The world's coastlines were then all shifted sea-
76 ward, e.g. ~ 3 – 25 km along the Andes, ~ 5 – 45 km along North Honshu, or ~ 15 – 45 km
77 along Cascadia, depending on the slope of the shelf (Ryan et al., 2009). Secondly, the
78 coastline of an uplifting active margin is erosive in essence: its location depends on the
79 competition between wave erosion and uplift (Bradley & Griggs, 1976; Anderson et al.,
80 1999). In short, coastlines are weak candidates to inform about tectonic processes as their

81 locations vary frequently due to non-tectonic factors. As a matter of fact, McNeill et al.
82 (2000) and Booth-Rea et al. (2008) noted that, in Cascadia, the outer arc high struc-
83 ture marking the edge of the continental shelf lies approximately above the downdip end
84 of coupling. The tectonic significance of active margin shelves thus merits to be inves-
85 tigated.

86 There is no unambiguous definition for *shelf* across geoscience communities. Here,
87 we understand shelf in a geomorphological context, i.e., the submarine domain affected
88 by wave-base erosion over cycles of low to high-stand, resulting in a more or less gen-
89 tle platform no deeper than 200 m below modern sea level (Bouma et al., 1982), a depth
90 that corresponds to 75 m (the reach of wave erosion) below the average lowstand level
91 (Seely & Dickinson, 1977). Contrary to passive margins where the shelf break is a strati-
92 graphic edifice whose location reflects the volume of sediment shed from continents (Bouma
93 et al., 1982), the shelf break of a subduction forearc is often pinned by tectonic defor-
94 mation (Seely & Dickinson, 1977; McNeill et al., 2000; Booth-Rea et al., 2008). Contrac-
95 tional and extensional strain caused by partial coupling between the overriding and down-
96 going plates are its primary drivers (Fuller et al., 2006; Wang & Hu, 2006; Cubas et al.,
97 2013; Noda, 2016). In fact, the shelf break frequently, but not always, coincides with the
98 position of the *outer arc high* (also described as *structural high* or *outer high*, Seely &
99 Dickinson, 1977). The outer arc high is often set by a thrust (blind or not) and gener-
100 ally marks the upper limit of the continental slope, where rocks begin to experience wave
101 base erosion (Seely & Dickinson, 1977; Anderson et al., 1999). Depending on its rela-
102 tive uplift rate, the shelf break is either the edge of an erosional platform or the seaward
103 sill (sometimes buried) of a forearc basin (Noda, 2016). Whether in a narrow erosive zone
104 (e.g. parts of the Andean subduction zone), or a complex domain with multiple deform-
105 ing basins trapped behind the outer arc (e.g. Cascadia), the shelf break is a clear topo-
106 graphic feature that is easily identifiable at almost all active margins regardless of their
107 structure (Seely & Dickinson, 1977; Noda, 2016). That said, we acknowledge exceptions
108 such as in the Alaska and the Colombia-Ecuador subduction zones where the foresets
109 of a depositional system mark the edge of the shelf (Bouma et al., 1982).

110 Since the compilation by Ruff and Tichelaar (1996), advances in geodetic inversions
111 for interseismic coupling and coseismic ruptures have allowed renewed scrutiny of po-
112 tential relationships between subduction zone coupling and coastal morphology. In this
113 article, we repeat the work of Ruff and Tichelaar (1996) with additional data; first with

114 well-resolved coseismic ruptures and second with solutions for both interseismic coupling
115 and the extent of large coseismic ruptures. To explore and illustrate the submarine ge-
116 omorphic expression of the location of the downdip end of coupling, we follow a simi-
117 lar path to that of Meade (2010) and compare patterns of erosion and of interseismic up-
118 lift. We observe that the edge of the continental shelf is a better first-order predictor of
119 the downdip end of high coupling than the originally proposed coastline. We develop a
120 model of wave erosion across a subduction margin where long-term vertical deformation
121 is partly driven by an uplift function resembling interseismic uplift, which is meant to
122 represent an anelastic fraction of deformation accumulated between large ruptures. We
123 show that the location of the shelf break can constrain the extent of the highly coupled
124 region integrated over many earthquake cycles in subduction zones.

125 **2 Apparent co-location of shelf break with the downdip end of seis-** 126 **mic coupling**

127 **2.1 Position of coseismic ruptures**

128 The amount of data constraining the downdip end of seismic ruptures and inter-
129 seismic coupling has increased in the two decades that followed the work of Ruff and Tichelaar
130 (1996), and warrants a new look at potential relations between landscape and seismo-
131 genic patterns. Figure 1 shows the outline of solutions for the downdip end of interseis-
132 mic coupling in Cascadia, and the downdip end of coseismic ruptures in Japan and Cen-
133 tral America. At the three locations, the downdip end of high coupling is broadly located
134 below the shelf break. These sites have shelves of width varying from about 25 to 75 km
135 (highlighted by the 200 m depth contour line).

136 The same co-location pattern can be observed in a global compilation of the region-
137 ally largest coseismic ruptures (Figure 2). This representation compares the respective
138 distances between downdip end of high coupling, shelf break, and coastline following and
139 expanding on the earlier work of Ruff and Tichelaar (1996). Following the terminology
140 introduced by Lay et al. (2012), large megathrust ruptures commonly slip across the highly
141 coupled zones A and/or B, which base marks the downdip end of high coupling (0 to ~35
142 km depth). To locate the downdip end of large earthquakes, we collected maps of large
143 coseismic ruptures for all major subduction systems. The downdip end of the rupture
144 patch solutions were exported to Google Earth (*kml* file available in the supplementary
145 material). In each subduction system, relative positions of the trench, the downdip end

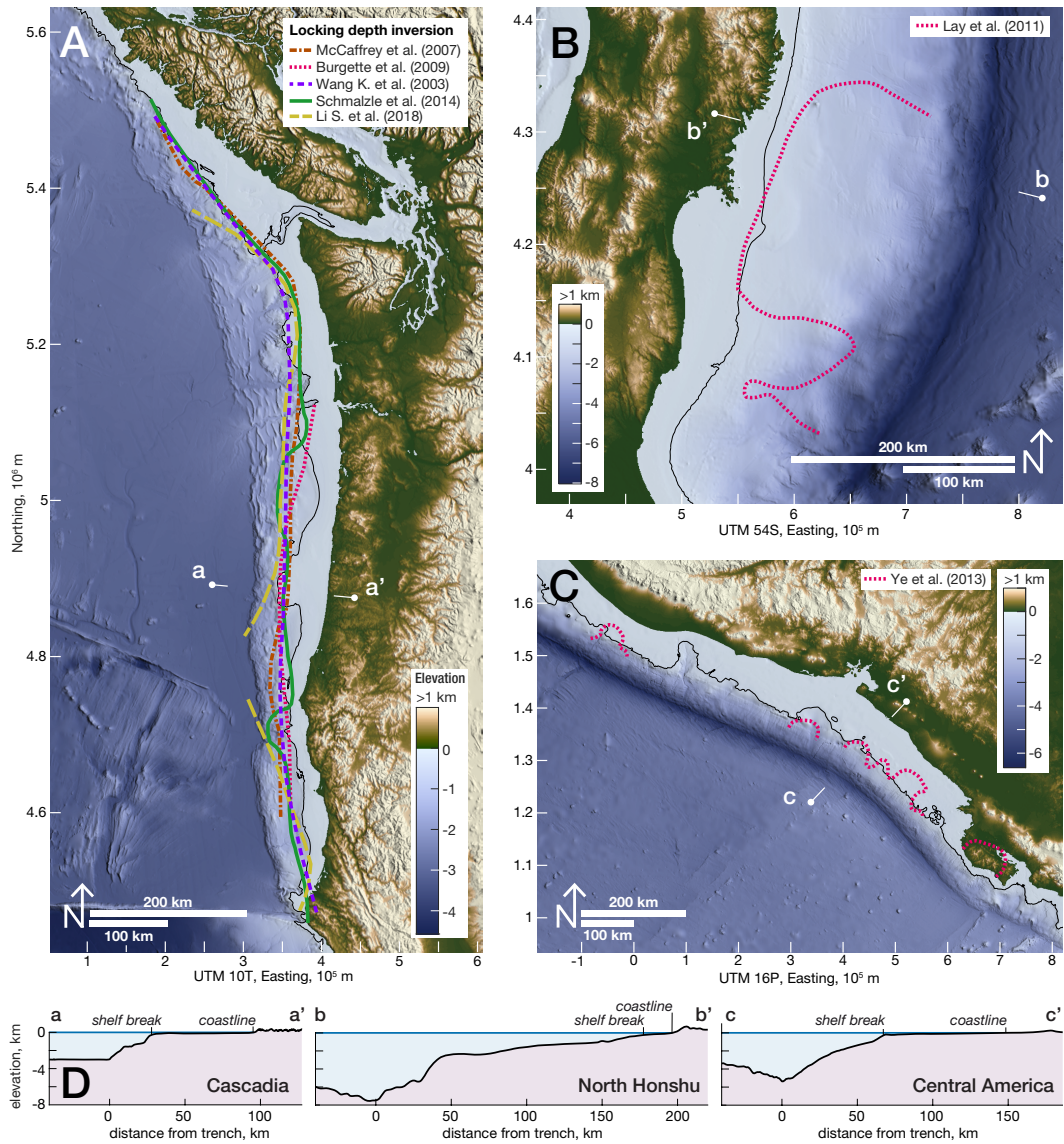


Figure 1: A: Solutions for the downdip end of interseismic coupling in Cascadia, derived from GPS (Wang et al., 2003; McCaffrey et al., 2007; Schmalzle et al., 2014; S. Li et al., 2018) and road leveling and tide gauges measurements (Burgette et al., 2009). The downdip end of high coupling is outlined for a value of $\sim 80\%$ coupling. B: Rupture extent of the M_w 9.1 Tōhoku-Oki earthquake (Lay et al., 2011). C: Rupture extent (at ~ 0.5 m displacement) of four Central American $M_w > 7$ megathrust earthquakes (Ye et al., 2013). The downdip ends of coupling and ruptures follow the edge of the continental shelf and are removed from the coastline. The black contour indicates 200 m depth, a common approximation for the geomorphic shelf edge. D: topographic profiles across the three margins; positions indicated by the opposite pins in the maps above. Topographic data from Ryan et al. (2009); color map from Crameri (2018).

146 of the rupture, the shelf break, and the coastline were measured. The shelf break is identified as the transition from the continental platform to the continental slope or, in the
 147 absence of clear features, pinned at ~ 200 m depth. For the sites where the shelf break
 148 is set by a structural feature and not by stratigraphic foresets, we observe (Figure 2 inset)
 149 is set by a structural feature and not by stratigraphic foresets, we observe (Figure 2 inset)
 150 set) that the mean position of the shelf breaks lie 1.13 km seaward of the downdip ends
 151 of rupture ($10^{\text{th}}/90^{\text{th}}$ percentiles at $-25.5/16$ km), while the coastlines lie landward at
 152 an average distance of 29.2 km ($10^{\text{th}}/90^{\text{th}}$ percentiles at $1/54$ km).

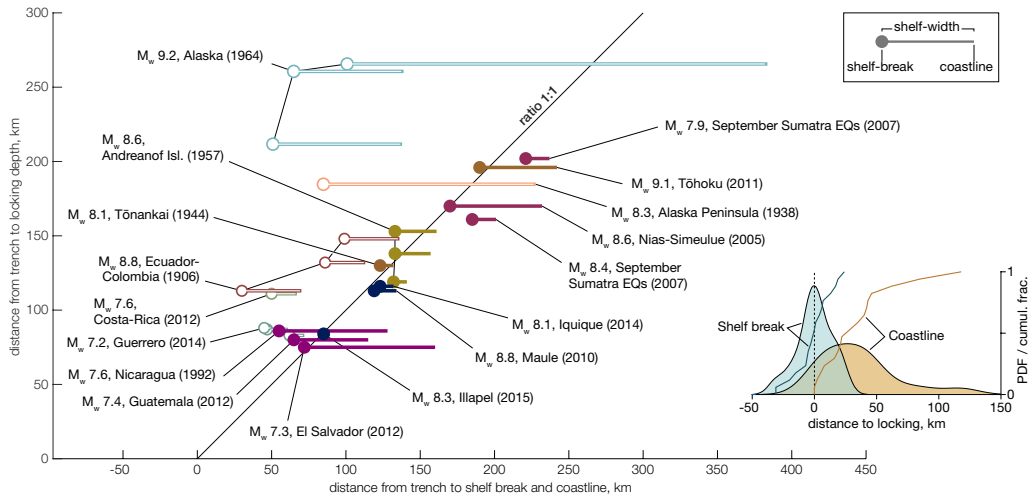


Figure 2: Position of the downdip edge of large megathrust earthquakes with respect to the local shelf break and coastline using the trench as origin (plot inspired by Ruff and Tichelaar (1996)). The inset kernel distribution shows the distance of shelf-edges and coastlines to the downdip edge of ruptures at sites marked with filled circles in the main plot (see text for rationale). Shelf breaks are tightly distributed around the downdip end of high coupling at a mean distance of -1.13 km ($10^{\text{th}}/90^{\text{th}}$ percentiles at $-25.5/16$ km) while coastlines are removed and spread landward from it at a mean distance of 29.2 km ($10^{\text{th}}/90^{\text{th}}$ percentiles at $1/54$ km). Sources are Sykes et al. (1981); Johnson (1998); Park et al. (2002); Cross and Freymueller (2007); Konca et al. (2008); Lay et al. (2011); Ye et al. (2013); Yue et al. (2014); Lay et al. (2014); Nocquet et al. (2014); L. Li et al. (2016).

2.2 Shelf break and downdip end of high coupling from co- and inter-seismic surveys.

The compilation can be further expanded with the inclusion of solutions for inter-seismic coupling that were developed with the advent of GPS monitoring (Larsen & Reilinger, 1992; Savage & Thatcher, 1992). A pattern similar to the co-location of shelf break and downdip end of rupture, albeit noisier, can be observed when interseismic coupling is included (Figure 3). To recover the position of the downdip end of high coupling, we collected maps of interseismic coupling for the major subduction systems. The downdip ends of highly coupled patches (using 80% coupling as a threshold) were exported to Google Earth (*kml* file available in the supplementary material). In each subduction system, relative positions of the trench, the downdip end of high coupling, the shelf break, and the coastline were measured along three to six profiles normal to the margin. Survey profiles were positioned to capture variability in relative positions of the coupling and morphological markers. The resulting 48 data points (coseismic and interseismic) are shown in Figure 3 A. This dataset includes all types of active margins, erosive shelf breaks but also depositional ones (sedimentary or volcanic, like Alaska or Kamchatka respectively); as well as locations with contradictory solutions for interseismic coupling that we had difficulties to reconcile (Chilean Andes, Nankai, and North Honshu all have multiple solutions stacked vertically in Figure 3 A). In order to compare similar settings and coupling patterns of high confidence, we further reduce the dataset to 21 sites by ignoring: interseismic constraints where good coseismic data is available (e.g. North Honshu); contradictory solutions for interseismic coupling (e.g. Chile); constructional shelf breaks set by the top of sedimentary foresets (Alaska, Ecuador-Colombia); or alternative solutions in sites where authors find equivalent patterns (Figure 3 B, details of the selection are in text S1 and Table S1 of the supplementary information). We also remove the Costa Rica subduction because of punctuated subduction erosion events that lead to transient changes in the accretionary prism geometry (Vannucchi et al., 2016). Finally, the Gorda subduction was also removed despite general overlap with Cascadia sites because of the amount of deformation accommodated by the very young oceanic crust itself as it subducts next to the Mendocino Triple Junction (Miller et al., 2001). The New Zealand North Island Hikurangi subduction does not appear in the compilation because of its low coupling (Wallace et al., 2004). The shelf breaks of the reduced set cluster around the downdip end of high coupling with a mean distance of 4.7 km landward and 10th and 90th per-

186 centiles at -18 and 22 km. Coastlines, in contrast, are shifted landward with a mean dis-
 187 tance of 43.1 km from the downdip end of high coupling and 10th and 90th percentiles
 188 at 3.2 and 76.6 km (Figure 3 B, inset). A similar but less tight distribution is observed
 189 in the complete dataset (Figure 3 A, inset).

190 A global compilation of the extent of seismicity $M_w \geq 5.5$ along megathrusts (Heuret
 191 et al., 2011) offers a promising alternative to the individual largest-earthquake inspec-
 192 tion we have done here (Figure 2). It would allow the statistical analysis of the surface
 193 morphology above the entire length of subduction zones, together with its seismogenic
 194 characteristics (Heuret et al., 2011), combined with a global slab geometry model (Hayes
 195 et al., 2018), and that regardless of the documented rupture of a large megathrust earth-
 196 quake.

197 Despite the diversity in the structure and morphology of active margins (as doc-
 198 umented in Noda, 2016), the edge of an erosive shelf is a markedly better predictor of
 199 the downdip end of coupling than the coastline. Indeed, already recognizing that the coast-
 200 line might not be a marker as reliable as they proposed, Ruff and Tichelaar (1996) noted
 201 that “continental shelf breaks [...] may have deeper physical significance [than the coast-
 202 line]”. Additionally, in Cascadia, McNeill et al. (2000) identified that the outer arc high,
 203 which marks the shelf break along this subduction, is co-located with the position of the
 204 downdip end of high coupling on the megathrust and Booth-Rea et al. (2008) noted that
 205 the seaward edge of the seismogenic transition lines up with the shelf break. In the next
 206 section, we discuss which processes control the landscape of active margins and under-
 207 lie the observed co-location of downdip end of high coupling and shelf break (Figures 2
 208 and 3).

209 **3 A model for active margin shelves**

210 The edge of active margin shelves appears to be a reliable guide for the position
 211 of the downdip end of high coupling on a megathrust (Figure 2 and 3). We propose here
 212 a conceptual model that can account for the observed colocation of the downdip end of
 213 seismic high coupling with the shelf break, and we illustrate this idea with a simple nu-
 214 merical model. If information about the coupling pattern of the megathrust is encoded
 215 in forearc morphology, it is crucial to A) identify all first-order drivers of long-term de-
 216 formation in order to isolate the signal that is solely related to the subduction zone seis-

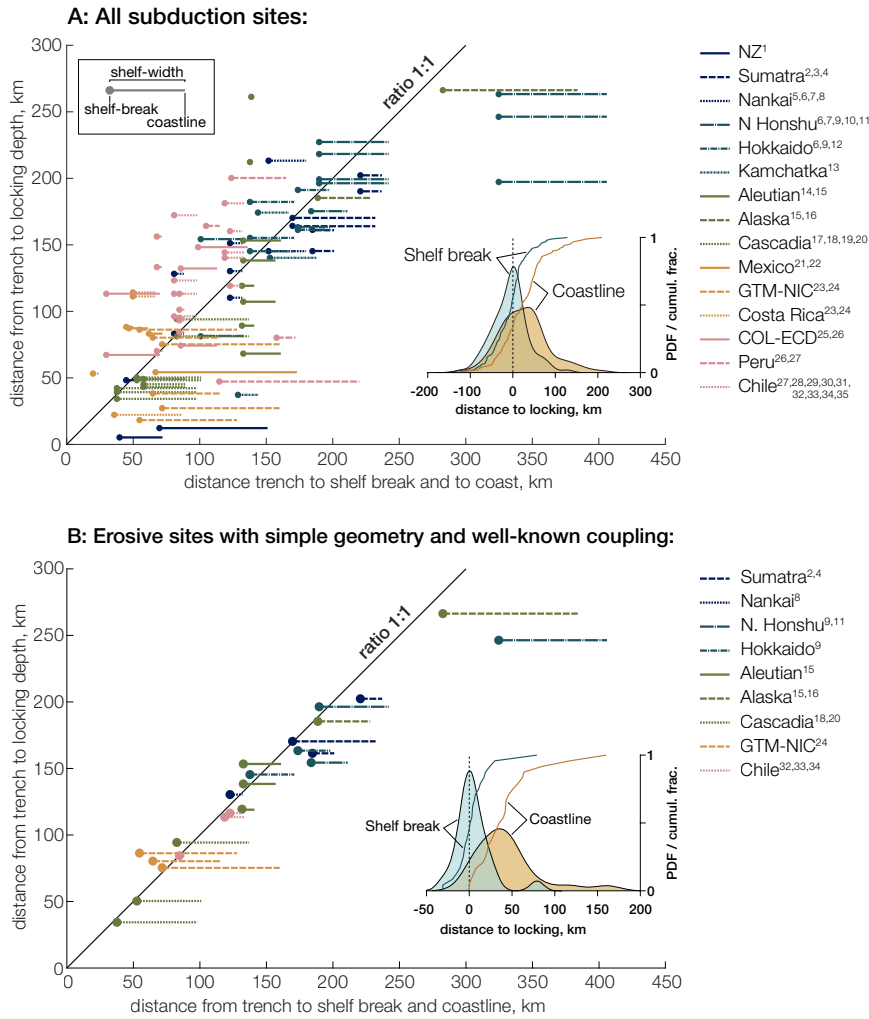


Figure 3: Position of the downdip end of high coupling with respect to the shelf break and the coastline relative to the trench (inspired by Ruff and Tichelaar (1996)). Left: compilation of all surveyed sites (locations with multiple coupling solutions are aligned vertically); right: compilation of sites with high confidence in downdip end of high coupling position and erosive shelf breaks. The inset distributions show that shelf breaks are clustered around the downdip end of high coupling while coastlines are shifted landward. For the indiscriminate compilation (top), the mean distance between shelf break and downdip end of high coupling is -6.18 km (10th/90th percentiles at -61.5/40 km), and 25.17 km between coastline and downdip end of high coupling (10th/90th percentiles of -43/93 km). For the high-confidence sites (bottom), the shelf breaks are tightly distributed at a mean distance of 4.7 km from the downdip end of high coupling (10th/90th percentiles at -18/22 km) while coastlines are shifted and spread landward from it at a mean distance of 43.1 km (10th/90th percentiles at 3.2/76.6 km). Caption continued on the next page.

Figure 3: Continued caption. Sources are 1: Wallace et al. (2004), 2: Natawidjaja et al. (2007), 3: Chlieh et al. (2008), 4: Briggs et al. (2006), 5: Hyndman et al. (1995), 6: Mazzotti et al. (2000), 7: Loveless and Meade (2010), 8: Park et al. (2002), 9: Hashimoto et al. (2009), 10: Simons et al. (2011), 11: Lay et al. (2011), 12: Sawai et al. (2004), 13: Bürgmann (2005), 14: Cross and Freymueller (2007), 15: Johnson (1998), 16: Sykes et al. (1981), 17: Wang et al. (2003), 18: Burgette et al. (2009), 19: McCaffrey et al. (2007), 20: Schmalzle et al. (2014), 21: Radiguet et al. (2012), 22: Franco et al. (2012), 23: LaFemina et al. (2009), 24: Ye et al. (2013), 25: Kanamori and McNally (1982), 26: Nocquet et al. (2014), 27: Chlieh et al. (2011), 28: Metois et al. (2012), 29: Metois et al. (2013), 30: Metois et al. (2016), 31: Béjar-Pizarro et al. (2013), 32: Lay et al. (2014), 33: Yue et al. (2014), 34: (L. Li et al., 2016), 35: (Saillard et al., 2017).

217 mic cycle and B) understand how this tectonic signal is encoded in the landscape mor-
 218 phology by erosive surface processes. The surface elevation of the lithosphere z evolves
 219 as a function of the total rock uplift rate U_{total} and the surface erosion rate E :

$$\frac{\partial z}{\partial t} = U_{\text{total}} - E. \quad (1)$$

220 To explore the morphological evolution of an active margin following Eq. 1, we turn to
 221 a simplified numerical model. We illustrate how coastlines get disconnected from tec-
 222 tonic structures and evaluate how much of the long-term uplift signal is expressed in fore-
 223 arc bathymetry when subjected to surface and seafloor shaping processes.

224 **3.1 Sources of active deformation in an active forearc**

225 We summarize tectonic deformation at subduction margins as the sum of three main
 226 components: 1) structural deformation from the growth of the forearc, 2) isostatic re-
 227 sponse to denudation or sedimentation at the surface and erosion or underplating at the
 228 megathrust, and 3) long-term deformation driven by the earthquake cycle (Figure 4).
 229 Together, they set the total rock uplift rate:

$$U_{\text{total}} = U_{\text{struct}} + U_{\text{iso}} + U_{\text{seismo}}. \quad (2)$$

230 Numerical models of coastal landscape evolution commonly use spatially uniform uplift
 231 (Anderson et al., 1999; Snyder et al., 2002; Melnick, 2016), but here the non-uniform field
 232 of uplift is key to understanding the reaction of the landscape and the stabilization of

233 the coastal domain. The relative magnitude of the three uplift components influences
 234 the co-location of the downdip end of high coupling and shelf break. In the absence of
 235 a mechanical model, we use arbitrary uplift profiles for structural and isostatic defor-
 236 mation, while the long-term seismic deformation is obtained from a back slip model.

237 ***3.1.1 Structural deformation from the growth of the forearc.***

238 Noda (2016) proposed a classification of forearcs that is particularly relevant for
 239 patterns of surface uplift or subsidence rates, U_{struct} , in the context of this study. Their
 240 structures can be organized along two axes: from extensional to contractional and from
 241 erosional to accretionary (with respect to mass fluxes across the subduction channel, not
 242 surface processes, von Huene & Lallemand, 1990; Clift & Vannucchi, 2004; Menant et
 243 al., 2020). Most forearc systems are either extensional and erosional *or* contractional and
 244 accretionary (Noda, 2016). The former are thinning and subsiding and tend to develop
 245 deep forearc basins whereas the latter are thickening and uplifting and have smaller basins
 246 or widespread surface erosion (Noda, 2016).

247 The structural uplift field that represents deformation of the forearc under exten-
 248 sion or contraction is drawn arbitrarily to represent the two end-member configurations
 249 under shortening (Figure 4 A) or extension (Figure 4 B). The structural deformation also
 250 encompasses thrusting in the accretionary wedge that would be necessary to counter-
 251 act interseismic subsidence seaward of the shelf break in order to stabilize the morphol-
 252 ogy of the continental slope.

253 ***3.1.2 Isostatic response to denudation and sedimentation.***

254 Another important component of rock uplift rate is the isostatic response U_{iso} to
 255 changes in the mass of the crust by surface erosion or deposition and by mass transfer
 256 across the megathrust (e.g. Lallemand et al., 1994; Braun et al., 2014). Coastal ranges
 257 are eroding and rock uplift should dominate landward while the offshore domain can be
 258 either erosive or aggradational depending on the forearc type, which leads to either up-
 259 lift or subsidence. Mass transfer by subduction erosion or underplating across the megath-
 260 rust can also significantly modify the mass of the crust and cause an isostatic response.

261 The isostatic response to denudation, sedimentation, and megathrust mass trans-
 262 fer is modeled as an arbitrary exponentially decaying uplift rate reaching zero at the trench

263 in the case of solely positive rock uplift primarily driven by denudation (Figure 4 A); to
 264 which a locus of subsidence centred around the forearc basin is added in the extensional
 265 case (Figure 4 B).

266 *3.1.3 Long-term deformation driven by the earthquake cycle.*

267 Although standard models of subduction seismic cycles assume elastic interseismic
 268 and coseismic deformation that perfectly balance each other (Savage, 1983), it is highly
 269 plausible that repeated cycles of deformation lead to some fraction of non-recoverable
 270 strain (e.g. King et al., 1988; Simpson, 2015). Permanent deformation can occur when-
 271 ever stresses reach the plastic envelope of the upper plate forearc. This can occur dy-
 272 namically at shallow depth during large seismic ruptures (e.g. Ma, 2012), or quasi-statically
 273 near the base of the coupled zone during interseismic loading (e.g. Vergne et al., 2001).
 274 The associated anelastic deformation mechanisms could include various processes of brittle
 275 rock fatigue, pressure-solution creep, or slip on pre-existing faults (Ashby & Sammis,
 276 1990; Niemeijer & Spiers, 2002; Paterson & Wong, 2005; Brantut et al., 2013). An ana-
 277 logue seismic cycle model that can reproduce both elastic and plastic deformation, with-
 278 out surface processes, effectively shows long-term uplift at and landward of the coast-
 279 line after the integration of multiple seismic cycles (Rosenau et al., 2009). In this frame-
 280 work, the net sum of each coseismic and interseismic deformation represents an incre-
 281 ment of permanent deformation, which, integrated over many cycles, shapes a specific
 282 pattern of long-term uplift and subsidence rates U_{seismo} of the forearc.

283 Lacking detailed observational or physical constraints on the exact shape of per-
 284 manent uplift and its relation to interseismic deformation but following the suggestion
 285 of Bilham et al. (1997), we postulate that the non-recoverable uplift that builds up over
 286 many seismic cycles represents a fraction of the vertical elastic displacement associated
 287 with the interseismic phase. This simplifying assumption allows us to model the shape
 288 of permanent uplift with the standard back slip approach (Savage, 1983; Kanda & Si-
 289 mons, 2010). Long-term interseismic rock uplift rates is computed with a back slip model
 290 (Savage, 1983) using half-space elastic Green's functions (Okada, 1992) and assuming
 291 a fully coupled region updip of the downdip end of high coupling and a transition zone
 292 downdip of it (see Bruhat & Segall, 2016, for details). The back slip model assumes that
 293 surface deformation is due to elastic strain accumulation on and around the plate inter-
 294 face and that it is equivalent to normal slip in the coupled region. We compute the dis-

295 tribution of interseismic surface uplift rates at an elevation of 0 m. Following estimates
 296 by Le Pichon et al. (1998), van Dinther et al. (2013), and Jolivet et al. (2020) we use a
 297 fraction (5%) of that deformation profile as a long-term field of uplift (Figure 5 A). It
 298 should be noted that without quantitative constraints on erosional efficiency, the abso-
 299 lute value of the uplift matters little while its spatial pattern is essential. The back slip
 300 model predicts a transition from subsidence (seaward) to uplift (landward), hereafter re-
 301 ferred to as hinge line, located within ca. 5 km of the downdip end of high coupling but
 302 that can also be displaced seaward with a gently dipping ($< 10^\circ$) slab and in the ab-
 303 sence of a transitional zone of partial coupling (supplementary Figure S1).

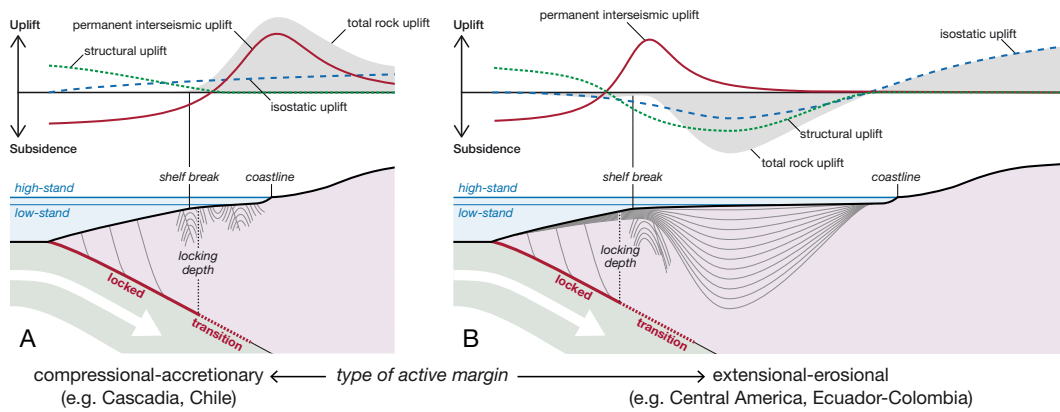


Figure 4: Conceptual model linking the morphology of active margins with the pattern of seismic coupling on the megathrust. A: contractional-accretionary forearc end-member (sensu Noda, 2016). The combined patterns of permanent interseismic, isostatic, and structural uplift set the edge of the erosive shelf, landward of which rock uplift exposes bedrock to wave-base erosion (top). The shelf break lies close to the location of the downdip edge of high coupling, pinned by the locally strong gradient in interseismic uplift. The shelf grows landward from the edge by coastal retreat (bottom). B: Extensional-erosional end-member (erosion refers to subduction erosion here). Here, subsidence of the wedge overcomes permanent interseismic uplift (top) and uplift at the shelf break acts as a sill for the forearc basin (bottom).

304

3.2 Sources of erosion

305

306

307

308

309

310

311

312

The morphology of active margins is primarily controlled by the competition between 1) uplift, 2) erosion, and 3) sediment aggradation and transport (Bradley & Griggs, 1976; Bouma et al., 1982; Anderson et al., 1999). We ignore subaerial erosion and sedimentation processes to focus on wave-base erosion. We adopt the phenomenological model of Anderson et al. (1999), which expends ocean wave energy on the shallow seafloor for wave-base erosion, leaving the remainder (if any) for sea-cliff erosion. First, offshore wave energy P_0 is expended and transformed into vertical erosion ($\partial z/\partial t$) depending on water depth h as the waves move closer to the shore:

$$\frac{\partial z}{\partial t} = \beta_z P_0 \exp\left(-\frac{4h}{h_{wb}}\right), \quad (3)$$

313

314

where β_z is an incision coefficient and h_{wb} is the depth of wave base. The remainder of the offshore energy is then transformed into a rate of cliff retreat $\partial x/\partial t$:

$$\frac{\partial x}{\partial t} = \beta_x \left[P_0 - \int_{shelf} P_0 \exp\left(-\frac{4h}{h_{wb}}\right) dx \right]. \quad (4)$$

315

316

317

318

319

320

321

The erosion component is driven by the sea level curve of Spratt and Lisiecki (2016) looped over 2 Myr for a naturally noisy eustatic signal. Wave energy is assumed constant through time. This is the best available code to investigate the first-order morphodynamics controlling eroding margins and it produces realistic looking topography. However, it can not be used to quantitatively invert a topographic profile and reconstruct either a history of uplift or sea-level as the two key coefficients β_x and β_z cannot be calibrated with more precision than a visual fit with non-unique parametrization allows.

322

3.3 Results

323

324

325

326

327

The uplift hinge line (separating seaward subsidence from landward uplift), acts as an anchor point for seafloor topography, which constantly evolves in response to wave base erosion. As illustrated below, the localization of this hinge-line above or near the downdip end of high coupling would result from the permanent, interseismic-like component of total rock uplift (Figure 5).

328

329

330

331

The effect of a localized peak of uplift driven by interseismic deformation appears critical in all types of forearc geometries (see Noda, 2016). For the contractional-accretionary end-member (Figure 4 A) the associated uplift peak marks the beginning of the domain where rocks are advected into the zone of wave-base erosion (and subaerial erosion land-

ward of the coast). For the extensional-erosional end-member, the interseismic uplift peak may not overcome structural and isostatic subsidence driven by extension and sedimentation but the peak can create a sill for the forearc basin by reducing subsidence locally (Figure 4 B). In both cases, the resulting structure would be compatible with an outer arc high (Seely & Dickinson, 1977; McNeill et al., 2000; Booth-Rea et al., 2008) and it would anchor a continental shelf that can grow landward by coastal erosion. The Matlab source code of the model is available in the supplementary material with a list of parameters to reproduce the simulations presented here along with three videos of the runs shown in Figure 5.

Wide erosive shelves

The morphology of wide, largely erosive, shelves of the Cascadia margin type (Figure 1) is characterized by a shelf break (corresponding to the outer arc high in Cascadia) above the downdip end of high coupling and a wide platform beveled by wave base erosion that displaced the coast landward (Figure 5 A). When wave energy is strong enough, and/or rock strength or uplift rate weak enough, the shelf can extend well beyond the peak of interseismic uplift. In this situation, the interseismic deformation signal recorded by onshore geodetic stations or surveys would reflect increasing interseismic uplift rates shoreward, as is the case in Cascadia (Burgette et al., 2009). Notably, landward of the uplift maximum, the erosion potential of wave energy enables an increasingly larger footprint as waves face slower uplift rates.

Wide subsiding shelves

In extensional-erosional active margins (subduction erosion) of the type found in Central America (Figure 1, Noda, 2016), the coastline is further removed from the shelf break by a subsiding basin. The model run of Figure 5 B illustrates this situation. For the incoming high-stand waves, the subsiding domain would have a relatively small energy cost limited to the transport of sediment on the shelf and wave-energy can be conserved over a large distance to erode the coast farther. The magnitude of interseismic deformation signals that could be picked up by onshore geodetic monuments is accordingly severely reduced. It should be noted that we are not modeling sedimentary dynamics here and that no energy expenditure is considered over the subsiding basin.

362

Narrow erosive shelves

363

364

365

366

367

368

369

370

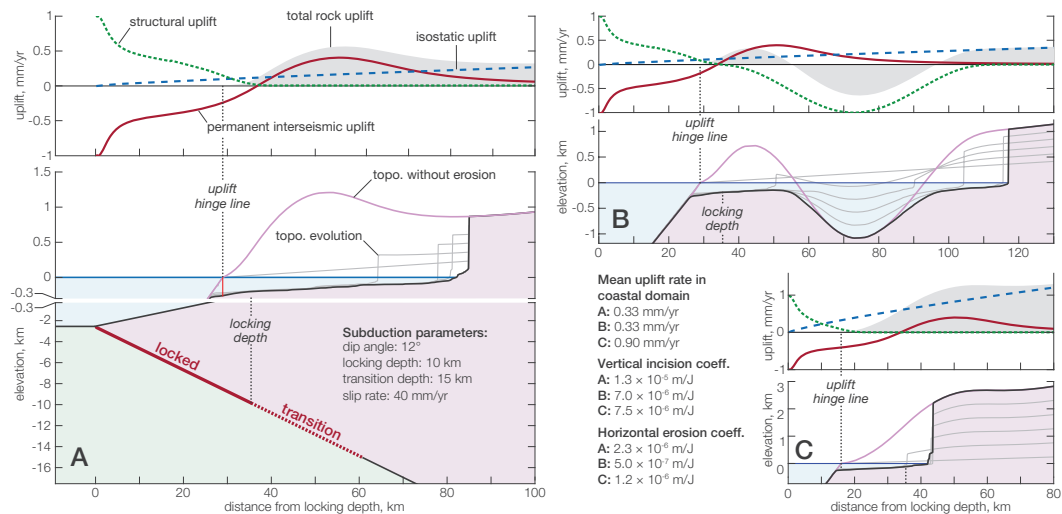


Figure 5: Numerical model illustrating the relationship between coastal morphology and subduction coupling patterns. Wave-base and cliff erosion following Anderson et al. (1999) are the only surface processes (no sedimentation, no subaerial erosion). Interseismic deformation is derived from the back slip model (adapted from Savage, 1983; Okada, 1992) of a strongly coupled fault. A: reference case with a wide shelf reflecting local uplift rates dominated by interseismic signature and relatively high rock erodibility. The vertical scale is exaggerated from -300 to 1000 m. B: subsidence of a forearc basin further separates shelf break and coastline. C: uplift rate is dominated by continental isostatic uplift and relatively low rock erodibility. In this case, the uplift hinge-line is significantly offset from the position of the downdip end of high coupling by the fast continental uplift. All models are run with the same subduction parameters and offshore wave energy. Videos for each of these runs are available in the supplementary material.

4 Perspectives and conclusion

4.1 Source of variability and commonalities in the compilation

Unlike the structural and isostatic components of uplift, the permanent seismic cycle component varies at short wavelength and is similar across subduction zones. It provides a straightforward connection between seismic cycle deformation and the morphology of the coastal domain. It is therefore a plausible candidate to explain the co-location of the downdip end of high coupling and the shelf break. Further investigating this idea will first require a mechanistic model for the spatial pattern of long-term permanent uplift. Interestingly, a growing body of observations suggests that it should resemble elastic deformation associated with the interseismic phase of the seismic cycle. For example, Allmendinger et al. (2009) noted that “at a regional scale within continents, interseismic deformation is mostly nearly similar to regional late Cenozoic tectonic deformation”. Work from Loveless and Allmendinger (2005) showed that the extensional strain field predicted by elastic interseismic deformation co-locates with regions of normal faulting in the Coastal Cordillera of Chile. Stevens and Avouac (2015) noted that the map of the uplift pattern predicted by seismic coupling on the Main Himalayan Thrust mimics the topography of the mountain range reflecting the agreements between 1) topography and GPS vertical motion (Bilham et al., 1997) and 2) fluvial incision and modelled interseismic uplift along a range-normal profile (Meade, 2010). Coastal uplift above subduction zones has also been partly attributed to interseismic deformation based on the pattern of deformed terraces in Cascadia (Kelsey & Bockheim, 1994; Personius, 1995); on the co-location of peninsulas and shallow downdip end of high coupling in the Andes (Saillard et al., 2017); on correlation between topography and interseismic uplift in northern Chile (Jolivet et al., 2020); and on the growth of the Japanese coastal mountains (Yoshikawa, 1968; Yoshikawa et al., 1981; Le Pichon et al., 1998). The analogue model for seismic cycles of Rosenau et al. (2009) also yields long-term uplift at the coastline. As this model does not include wave erosion, the modelled coastline is located at the uplift hinge line, i.e., where the erosive shelf break would be located if erosion was to push the coast landwards.

Most subduction zones share a common pattern with more or less homogeneous seismic coupling in the upper part of the megathrust and creep in the lower part (e.g. Lay et al., 2012). The permanent deformation derived from interseismic loading can then

403 be reasonably expected to follow a largely similar pattern from one strongly coupled megathrust to another: subsidence above the seaward (shallower) seismic coupling, and uplift
404 above the landward (deeper) creeping portion. This pattern is insensitive to the root cause
405 of the downdip end of high coupling, whether it reflects a thermal or lithological threshold (e.g., moho of the upper plate, Hyndman et al., 1997). By contrast, the pattern of
406 isostatic uplift or subsidence is expected to vary according to the regimes of denudation
407 and deposition but to retain an overall similarity with more uplift landward and less (or
408 more negative) uplift seaward. In this framework, the large structural and morphological
409 diversity of forearc basins mainly stems from the forearc deformation set by its mass
410 balance (erosional vs. accretionary, Noda, 2016).
411

412
413 The scatter around the position of the downdip end of high coupling in Figure 2
414 and 3 may result from a combination of factors, chiefly among them uncertainties in the
415 inversion of interseismic coupling and coseismic ruptures, and differences between the
416 pattern of anelastic versus elastic interseismic deformation. The use of an elastic or viscoelastic model to identify the downdip end of high coupling may also affect its position.
417 In Cascadia, the extent of high coupling is somewhat shallower with a viscoelastic model
418 (S. Li et al., 2018) but not significantly different (Figure 1). However the uplift hinge
419 line modelled by S. Li et al. (2018) lies closer to the coastline than predictions of elastic
420 models for the same margin. Yet, regardless of the inversion method employed, the
421 lack of submarine geodetic data will affect the modelled location of the interseismic downdip
422 end of high coupling and the position of the modelled uplift hinge line (S. Li et al., 2018).
423 The relative magnitudes of the three uplift components can alter the relationship between
424 downdip end of high coupling and shelf break. This is illustrated by the model run of
425 Figure 5 C where isostatic deformation dominates the total uplift.
426

427 **4.2 Critical taper and other modes of deformation**

428 Critical taper theory (Dahlen, 1984) is essential to explain the full deformation pattern of active margins (here named *structural uplift*). It could also provide an alternative explanation for the pattern of deformation that we ascribe to permanent interseismic deformation. The deformation pattern of a critical wedge changes in response to variations in basal friction such that a vertical shear zone marking the onset of landward uplift could localize above the downdip end of high coupling (Fuller et al., 2006; Cubas et al., 2013). However, for this hinge line to develop, the wedge has to be critical, which
434

435 is a condition only met in parts of a few subduction zones (Cubas et al., 2013; Rousset
436 et al., 2016; Koulali et al., 2018). Given the limited occurrence of critically tapered sub-
437 duction zones globally, we find that anelastic interseismic deformation provides a more
438 plausible explanation for the global signal of downdip ends of high coupling revealed by
439 coastal geomorphology (Figure 3). Nevertheless, if uplift at the shelf break is not caused
440 by permanent interseismic deformation as we argue here, it is likely that its connection
441 to the regime of coupling on the megathrust could be elucidated by looking at patterns
442 of internal deformation of critical wedges.

443 Large deep earthquakes in the partially coupled zone C *sensu* Lay et al. (2012), i.e.
444 deeper than the downdip end of high coupling (~ 35 to ~ 55 km), have been recorded as
445 well (e.g., Lay et al., 2012; Schurr et al., 2012; Moreno et al., 2018). These rare ruptures
446 have been proposed to drive coastal uplift in the Central Andes by Melnick (2016). In
447 this hypothesis, the coseismic uplift of earthquakes in the shallower coupled zones A and
448 B would be compensated by subsidence during the post- and interseismic periods, un-
449 like their rarer and deeper zone C counterparts. It is unclear why this deep coseismic
450 component alone is not compensated and why it would be the driver of permanent seis-
451 mogenic deformation at subduction margins while much greater seismogenic slip occurs
452 on fully coupled zones A and B (Lay et al., 2012).

453 Mouslopoulou et al. (2016) propose that coseismic slip on upper plate faults clus-
454 tered around the coastline is responsible for coastal uplift rather than interseismic de-
455 formation. The hypothesis is driven by observation of uplift transients mainly based on
456 an extensive radiocarbon age dataset of marine terrace in Crete (Mouslopoulou et al.,
457 2015). The samples of the Cretan dataset were however shown to be likely radiocarbon
458 dead with varying amount of secondary contamination controlling the apparent age by
459 Ott et al. (2019) who compared them to independent luminescence dating. The idea of
460 rapid uplift transients driven by the magnitude-frequency distribution of earthquakes (Mouslopoulou
461 et al., 2016) may still hold if the bulk uplift near the coast is aseismic and its short-term
462 variability is modulated by earthquakes along the megathrust and in the upper plate.

463 Our modeling focuses on the interaction between uplift and wave-base erosion that
464 shapes the continental shelf. We do not address the subsiding parts of the margin. How-
465 ever, observations of deformation and sedimentation in zones of interseismic subsidence
466 support our assumption and complements our work on the erosive part of the system.

467 The strongly coupled domain of megathrusts has been observed to be often overlain by
 468 large forearc basins on deep sea terraces seaward of the shelf (Sugiyama, 1994; Song &
 469 Simons, 2003; Wells et al., 2003). These deep subsiding forearc basins have been attributed
 470 to subduction erosion (Wells et al., 2003), and to critical taper deformation of the in-
 471 ner wedge (Fuller et al., 2006; Wang & Hu, 2006; Cubas et al., 2013). If these forearc
 472 basins are indeed the depositional counterparts of erosive shelves and are driven by long-
 473 term interseismic deformation, then their stratigraphy could inform the temporal sta-
 474 bility of the coupling pattern in a manner that erosion on the shelf cannot.

475 4.3 A bridge between seismic and landscape timescales

476 Geodetic measurements of interseismic coupling or coseismic ruptures reflect at most
 477 a few centuries of geological history. Meanwhile, the landscape records the effect of tec-
 478 tonics and surface processes over hundreds to thousands of individual seismic cycles span-
 479 ning 100's of kyrs (e.g. Valensise & Ward, 1991; Willett et al., 1993; Lavé & Avouac, 2001;
 480 Avouac, 2003; Meade, 2010). Hence, if the position of the downdip end of high coupling
 481 is stable — as expected from a fault with a characteristic earthquake cycle, where the
 482 region strongly coupled during the interseismic period exactly delimits the extent of fu-
 483 ture earthquakes — the same domains are in net rock subsidence or rock uplift 100% of
 484 the time and the shelf break should be a sharp morphological marker (like in Cascadia
 485 potentially, Figure 6).

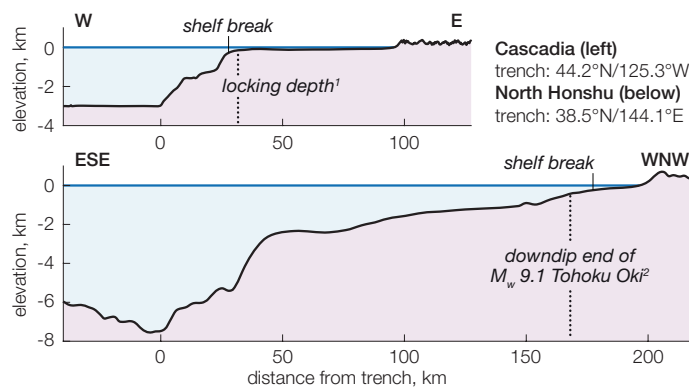


Figure 6: Profiles across the Cascadia and North Honshu margins. In Cascadia, the shelf break is a sharp and salient feature while in North Honshu the shelf break is lost in the upper continental slope. Both figures share the same scale. 1: Burgette et al. (2009); 2: Lay et al. (2011). Topographic data from Ryan et al. (2009).

486 While the assumption of a characteristic earthquake cycle is common, interseismic
487 coupling might also plausibly vary over several seismic cycles, leading to a more poorly
488 defined shelf break (such as observed in Japan, Figure 6) because the transition from sub-
489 siding all of the time to uplifting all of the time would not be well defined spatially . Ad-
490 ditionally, within the interseismic period itself, there is increasing evidence that coupling
491 distribution could be time-dependent. The downdip end of coupling could migrate up-
492 dip during the interseismic period, resulting in variable degrees of possible mismatch be-
493 tween coseismic reconstructions and current interseismic measurements (Thatcher, 1984;
494 Schmalzle et al., 2014; Nishimura, 2014; Jiang & Lapusta, 2016; Wang & Tréhu, 2016;
495 Bruhat & Segall, 2017).

496 Beyond temporal variations, the pattern of long-term uplift depends as much on
497 the spatial distribution of interseismic deformation as on that of coseismic displacement.
498 Coseismic deformation can also locally overcome interseismic deformation when splay
499 faults focus the former in a narrower domain as in Sumatra (Sieh et al., 2008; Philibosian
500 et al., 2014) or in South-Central Chile (Bookhagen et al., 2006). The respective spatial
501 distributions of co- and interseismic deformation may also differ on large scale (Penserini
502 et al., 2017). Fast (coseismic) or slow (interseismic) deformation can be discriminated
503 with the characteristic signatures they may leave in the geological record under specific
504 conditions. Provided sufficient sudden uplift relative to local tidal range and wave en-
505 ergy, a submarine surface can be brought out of the wave erosion domain, promoting its
506 preservation (e.g. in Sumatra, Sieh et al., 2008). Alternatively, coastal ecosystems can
507 be suddenly drowned and preserved after sufficient coseismic subsidence (e.g. in Casca-
508 dia, Atwater, 1987). Meanwhile, the rate of interseismic deformation is comparable to
509 that of different erosive and depositional surface processes that can keep up with it. The
510 model proposed here opens the exploration of long-term stability or transience of inter-
511 seismic coupling patterns.

512 **4.4 Conclusion**

513 We observe that the edge of a subduction margin shelf is a markedly better indi-
514 cator of the downdip end of high coupling on the megathrust than the coastline. We pro-
515 pose that this co-location directly results from the pattern of permanent interseismic de-
516 formation that drives a relative peak in uplift rate just landward of the downdip edge
517 of high coupling. We show that a model combining permanent deformation that mim-

518 ics interseismic uplift with wave-base erosion reproduces the first order alignment of shelf
 519 breaks above the seismic downdip ends of high coupling of subduction megathrusts, as
 520 observed in a global survey. We present a first-order relationship between active mar-
 521 gin morphology and seismogenic patterns at depth. This proposition calls for future val-
 522 idation in the form of mechanical modeling and field observations. The morphological
 523 expression of the seismogenic characteristics of a megathrust is particularly valuable where
 524 shelves are wide and onshore geodetic surveys accordingly limited. The submarine land-
 525 scape of an active margin integrates repeated seismic cycles and bridges seismic timescales
 526 (100's of yrs) with those of landscape building (100's of kyrs). As a result, the stabil-
 527 ity or transience of seismic coupling would be recorded in the morphology of the shelf
 528 break itself.

529 **Acknowledgments**

530 We thank Jean-Philippe Avouac, Emily Brodsky, Nadaya Cubas, Cécile Lasserre, Thorne
 531 Lay, Marianne Métois, and Baptiste Rousset for stimulating discussions. We thank Jack
 532 Loveless and Onno Oncken for their constructive reviews along Associate Editor Ylona
 533 van Dinther. We also acknowledge the remarks of three anonymous reviewers. Malat-
 534 esta was supported by a Post.Doc Mobility fellowship of the Swiss National Science Foun-
 535 dation (P2SKP2_168328). Bruhat has received funding from the People Programme (Marie
 536 Curie Actions) of the European Unions Seventh Framework Programme (FP7/2007-2013)
 537 under REA grant agreement n. PCOFUND-GA-2013-609102, through the PRESTIGE
 538 programme coordinated by Campus France. Olive was supported by an Emergence(s)
 539 – Ville de Paris grant. All information supporting this contribution is present in the main
 540 manuscript or the supplementary material. The MATLAB code for the numerical model
 541 as well as the compilation of locations are available in the Supplementary Information.

542 **References**

- 543 Aki, K. (1967). Scaling law of seismic spectrum. *Journal of Geophysical Research:*
 544 *Planets*, 72(4), 1217–1231.
- 545 Allmendinger, R. W., Loveless, J. P., Pritchard, M. E., & Meade, B. (2009, Novem-
 546 ber). From decades to epochs: Spanning the gap between geodesy and struc-
 547 tural geology of active mountain belts. *Journal Of Structural Geology*, 31(11),
 548 1409–1422.
- 549 Anderson, R. S., Densmore, A. L., & Ellis, M. A. (1999, March). The generation and

- 550 degradation of marine terraces. *Basin Research*, 11(1), 7–19.
- 551 Ashby, M. F., & Sammis, C. G. (1990). The Damage Mechanics of Brittle Solids in
552 Compression. *Pure and Applied Geophysics*, 133(3), 489–521.
- 553 Atwater, B. F. (1987). Evidence for great holocene earthquakes along the outer
554 coast of washington state. *Science*, 236(4804), 942–944. doi: 10.1126/science
555 .236.4804.942
- 556 Avouac, J.-P. (2003). Mountain building, erosion, and the seismic cycle in the Nepal
557 Himalaya. *Advances in Geophysics*.
- 558 Béjar-Pizarro, M., Socquet, A., Armijo, R., Carrizo, D., Genrich, J., & Simons, M.
559 (2013, April). Andean structural control on interseismic coupling in the North
560 Chile subduction zone. *Nature Geoscience*, 6(6), 462–467.
- 561 Bilham, R., Larson, K., & Freymueller, J. (1997). Gps measurements of present-day
562 convergence across the nepal himalaya. *Nature*, 386(6620), 61–64.
- 563 Bookhagen, B., Echtler, H. P., Melnick, D., Strecker, M. R., & Spencer, J. Q. G.
564 (2006). Using uplifted holocene beach berms for paleoseismic analysis on the
565 santa mara island, south-central chile. *Geophysical Research Letters*, 33(15).
566 doi: 10.1029/2006GL026734
- 567 Booth-Rea, G., Klaeschen, D., Grevemeyer, I., & Reston, T. (2008, July). Hetero-
568 geneous deformation in the Cascadia convergent margin and its relation to
569 thermal gradient (Washington, NW USA). *Tectonics*, 27(4), 1–15.
- 570 Bouma, A. H., Berryhill, H. L., Brenner, R. L., & Knebel, H. J. (1982, January).
571 Continental Shelf and Epicontinental Seaways. *Sandstone Depositional Envi-
572 ronments*, 31, 0.
- 573 Bradley, W. C., & Griggs, G. B. (1976, March). Form, genesis, and deformation of
574 central California wave-cut platforms. *Geological Society of America Bulletin*,
575 87(3), 433–449.
- 576 Brantut, N., Heap, M. J., Meredith, P. G., & Baud, P. (2013, July). Time-
577 dependent cracking and brittle creep in crustal rocks: A review. *Journal
578 Of Structural Geology*, 52(C), 17–43.
- 579 Braun, J., Simon-Labric, T., Murray, K. E., & Reiners, P. W. (2014, June). Topo-
580 graphic relief driven by variations in surface rock density. *Nature Geoscience*.
- 581 Briggs, R. W., Sieh, K., Meltzner, A. J., Natawidjaja, D. H., Galetzka, J., Suwar-
582 gadi, B. W., . . . Bock, Y. (2006). Deformation and slip along the Sunda

- 583 Megathrust in the great 2005 Nias-Simeulue earthquake. *Science*, 311(5769),
584 1897–1901.
- 585 Brooks, B. A., Bevis, M., Whipple, K., Arrowsmith, J. R., Foster, J., Zapata, T., ...
586 Smalley, R. J. (2011, May). Orogenic-wedge deformation and potential for
587 great earthquakes in the central Andean backarc. *Nature Geoscience*, 4(6),
588 380–383.
- 589 Bruhat, L., & Segall, P. (2016, November). Coupling on the northern Cascadia sub-
590 duction zone from geodetic measurements and physics-based models. *Journal*
591 *of Geophysical Research*, 121(11), 8297–8314.
- 592 Bruhat, L., & Segall, P. (2017, July). Deformation rates in northern Cascadia consis-
593 tent with slow updip propagation of deep interseismic creep. *Geophysical Jour-*
594 *nal International*, 211(1), 427–449.
- 595 Burgette, R. J., Weldon II, R. J., & Schmidt, D. A. (2009, January). Interseis-
596 mic uplift rates for western Oregon and along-strike variation in locking on
597 the Cascadia subduction zone. *Journal of Geophysical Research*, 114(B1),
598 TC3009–24.
- 599 Bürgmann, R. (2005). Interseismic coupling and asperity distribution along the
600 Kamchatka subduction zone. *Journal of Geophysical Research*, 110(B7), 1675–
601 17.
- 602 Bürgmann, R., & Chadwell, D. (2014, May). Seafloor Geodesy. *Annual Review Of*
603 *Earth And Planetary Sciences*, 42(1), 509–534.
- 604 Chlieh, M., Avouac, J.-P., Sieh, K., Natawidjaja, D. H., & Galetzka, J. (2008, May).
605 Heterogeneous coupling of the Sumatran megathrust constrained by geodetic
606 and paleogeodetic measurements. *Journal of Geophysical Research-Solid Earth*
607 *and Planets*, 113(B5), 2018–31.
- 608 Chlieh, M., Perfettini, H., Tavera, H., Avouac, J.-P., Remy, D., Nocquet, J.-M., ...
609 Bonvalot, S. (2011, December). Interseismic coupling and seismic potential
610 along the Central Andes subduction zone. *Journal of Geophysical Research*,
611 116(B12), B10404–21.
- 612 Clift, P., & Vannucchi, P. (2004). Controls on tectonic accretion versus erosion in
613 subduction zones: Implications for the origin and recycling of the continental
614 crust. *Reviews of Geophysics and Space Physics*, 42(2), 1–31.
- 615 Cramer, F. (2018). Geodynamic diagnostics, scientific visualisation and StagLab

- 616 3.0. *Geoscientific Model Development*, 11(6), 2541–2562.
- 617 Cross, R. S., & Freymueller, J. T. (2007, March). Plate coupling variation and block
618 translation in the Andreanof segment of the Aleutian arc determined by sub-
619 duction zone modeling using GPS data. *Geophysical Research Letters*, 34(6),
620 1653–5.
- 621 Cubas, N., Avouac, J.-P., Souloumiac, P., & Leroy, Y. (2013, November). Megath-
622 rust friction determined from mechanical analysis of the forearc in the Maule
623 earthquake area. *Earth and Planetary Science Letters*, 381(C), 92–103.
- 624 Dahlen, F. A. (1984). Noncohesive Critical Coulomb Wedges - an Exact Solution.
625 *Journal of Geophysical Research*, 89, 125–133.
- 626 Dragert, H., Wang, K. L., & James, T. S. (2001). A silent slip event on the deeper
627 Cascadia subduction interface. *Science*, 292(5521), 1525–1528.
- 628 Franco, A., Lasserre, C., Lyon-Caen, H., Kostoglodov, V., Molina, E., Guzman-
629 Speziale, M., . . . Manea, V. C. (2012, April). Fault kinematics in northern
630 Central America and coupling along the subduction interface of the Cocos
631 Plate, from GPS data in Chiapas (Mexico), Guatemala and El Salvador. *Geo-
632 physical Journal International*, 189(3), 1223–1236.
- 633 Fuller, C., Willett, S. D., & Brandon, M. T. (2006). Formation of forearc basins and
634 their influence on subduction zone earthquakes. *Geology*, 34(2), 65–68.
- 635 Hashimoto, C., Noda, A., Sagiya, T., & Matsu'ura, M. (2009, January). Interplate
636 seismogenic zones along the Kuril-Japan trench inferred from GPS data inver-
637 sion. *Nature Geoscience*, 2(2), 141–144.
- 638 Hayes, G. P., Moore, G. L., Portner, D. E., Hearne, M., Flamme, H., Furtney, M.,
639 & Smoczyk, G. M. (2018). Slab2, a comprehensive subduction zone geometry
640 model. *Science*, 362(6410), 58–61. doi: 10.1126/science.aat4723
- 641 Heuret, A., Lallemand, S., Funicello, F., Piromallo, C., & Faccenna, C. (2011).
642 Physical characteristics of subduction interface type seismogenic zones re-
643 visited. *Geochemistry, Geophysics, Geosystems*, 12(1). doi: 10.1029/
644 2010GC003230
- 645 Hyndman, R. D., Wang, K., & Yamano, M. (1995, August). Thermal constraints on
646 the seismogenic portion of the southwestern Japan subduction thrust. *Journal
647 of Geophysical Research: Planets*, 100(B8), 15373–15392.
- 648 Hyndman, R. D., Yamano, M., & Oleskevich, D. A. (1997). The seismogenic zone of

- 649 subduction thrust faults. *Island Arc*, 6(3), 244-260. doi: 10.1111/j.1440-1738
 650 .1997.tb00175.x
- 651 James, T. S., Gowan, E. J., Wada, I., & Wang, K. (2009, April). Viscosity of the
 652 asthenosphere from glacial isostatic adjustment and subduction dynamics at
 653 the northern Cascadia subduction zone, British Columbia, Canada. *Journal of*
 654 *Geophysical Research-Solid Earth and Planets*, 114(B4), 536–13.
- 655 Jiang, J., & Lapusta, N. (2016, June). Deeper penetration of large earthquakes on
 656 seismically quiescent faults. *Science*, 352(6291), 1293–1297.
- 657 Johnson, J. M. (1998). Heterogeneous Coupling Along Alaska-Aleutians as Inferred
 658 From Tsunami, Seismic, and Geodetic Inversions. In *Tsunamigenic earthquakes*
 659 *and their consequences* (pp. 1–116). Elsevier.
- 660 Jolivet, R., Simons, M., Duputel, Z., Olive, J.-A., Bhat, H. S., & Bletery, Q. (2020).
 661 Interseismic loading of subduction megathrust drives long-term uplift in
 662 northern Chile. *Geophysical Research Letters*, 47(8), e2019GL085377. doi:
 663 10.1029/2019GL085377
- 664 Kanamori, H., & McNally, K. C. (1982, August). Variable rupture mode of the sub-
 665 duction zone along the Ecuador-Colombia coast. *Bulletin of the Seismological*
 666 *Society of America*, 72(4), 1241–1253.
- 667 Kanda, R. V. S., & Simons, M. (2010). An elastic plate model for interseismic
 668 deformation in subduction zones. *Journal of Geophysical Research: Planets*,
 669 115(B3), 2328.
- 670 Kelsey, H. M., & Bockheim, J. G. (1994, June). Coastal landscape evolution as a
 671 function of eustasy and surface uplift rate, Cascadia margin, southern Oregon.
 672 *Geological Society of America Bulletin*, 106(6), 840–854.
- 673 King, G. C. P., Stein, R. S., & Rundle, J. B. (1988). The Growth of Geological
 674 Structures by Repeated Earthquakes .1. Conceptual-Framework. *Journal of*
 675 *Geophysical Research*, 93, 13307–13318.
- 676 Konca, A. O., Avouac, J.-P., Sladen, A., Meltzner, A. J., Sieh, K., Fang, P., ...
 677 Helmberger, D. (2008, December). Partial rupture of a locked patch of the
 678 Sumatra megathrust during the 2007 earthquake sequence. *Nature*, 456(7222),
 679 631–635.
- 680 Koulali, A., McClusky, S., Cummins, P., & Tregoning, P. (2018, June). Wedge ge-
 681 ometry, frictional properties and interseismic coupling of the Java megathrust.

- 682 *Tectonophysics*, 734-735, 89–95.
- 683 LaFemina, P., Dixon, T. H., Govers, R., Norabuena, E., Turner, H., Saballos, A.,
684 ... Strauch, W. (2009, May). Fore-arc motion and Cocos Ridge collision in
685 Central America. *Geochemistry Geophysics Geosystems*, 10(5), n/a–n/a.
- 686 Lallemand, S. E., Schnrle, P., & Malavieille, J. (1994). Coulomb theory applied
687 to accretionary and nonaccretionary wedges: Possible causes for tectonic ero-
688 sion and/or frontal accretion. *Journal of Geophysical Research: Solid Earth*,
689 99(B6), 12033-12055. doi: 10.1029/94JB00124
- 690 Larsen, S., & Reilinger, R. (1992, June). Global positioning system measurements of
691 strain accumulation across the Imperial Valley, California: 1986–1989. *Journal*
692 *of Geophysical Research: Planets*, 97(B6), 8865–8876.
- 693 Lavé, J., & Avouac, J.-P. (2001, January). Fluvial incision and tectonic uplift across
694 the Himalayas of central Nepal. *Journal of Geophysical Research*, 106(B11),
695 26561–26,591.
- 696 Lay, T., Ammon, C. J., Kanamori, H., Xue, L., & Kim, M. J. (2011, September).
697 Possible large near-trench slip during the 2011 M_w 9.0 off the Pacific coast of
698 Tohoku Earthquake. *Earth, Planets and Space*, 63(7), 687–692.
- 699 Lay, T., Kanamori, H., Ammon, C. J., Koper, K. D., Hutko, A. R., Ye, L., ... Rush-
700 ing, T. M. (2012, April). Depth-varying rupture properties of subduction zone
701 megathrust faults. *Journal of Geophysical Research*, 117(B4), n/a–n/a.
- 702 Lay, T., & Schwartz, S. Y. (2004). Comment on “coupling semantics and science in
703 earthquake research”. *Eos, Transactions American Geophysical Union*, 85(36),
704 339-340. doi: 10.1029/2004EO360003
- 705 Lay, T., Yue, H., Brodsky, E. E., & An, C. (2014, June). The 1 April 2014 Iquique,
706 Chile, M_w 8.1 earthquake rupture sequence. *Geophysical Research Letters*,
707 41(11), 3818–3825.
- 708 Le Pichon, X., Mazzotti, S., Henry, P., & Hashimoto, M. (1998, August). Deforma-
709 tion of the Japanese Islands and seismic coupling: an interpretation based on
710 GSI permanent GPS observations. *Geophysical Journal International*, 134(2),
711 501–514.
- 712 Li, L., Lay, T., Cheung, K. F., & Ye, L. (2016, May). Joint modeling of teleseismic
713 and tsunami wave observations to constrain the 16 September 2015 Illapel,
714 Chile, M_w 8.3 earthquake rupture process. *Geophysical Research Letters*, 43(9),

- 715 4303–4312.
- 716 Li, S., Wang, K., Wang, Y., Jiang, Y., & Dosso, S. E. (2018). Geodetically in-
717 ferred locking state of the cascadia megathrust based on a viscoelastic earth
718 model. *Journal of Geophysical Research: Solid Earth*, *123*(9), 8056–8072. doi:
719 10.1029/2018JB015620
- 720 Loveless, J. P., & Allmendiger, R. W. (2005). Implications of elastic dislocation
721 modeling on permanent deformation in the Northern Chilean forearc. In *Inter-*
722 *national symposium on andean geodynamics* (pp. 454–457). Barcelona.
- 723 Loveless, J. P., & Meade, B. J. (2010, February). Geodetic imaging of plate mo-
724 tions, slip rates, and partitioning of deformation in Japan. *Journal of Geophys-*
725 *ical Research*, *115*(B2), L11303–35.
- 726 Ma, S. (2012, June). A self-consistent mechanism for slow dynamic deformation and
727 tsunami generation for earthquakes in the shallow subduction zone. *Geophys-*
728 *ical Research Letters*, *39*(11), n/a–n/a.
- 729 Mai, P. M., & Beroza, G. C. (2000, June). Source Scaling Properties from Finite-
730 Fault-Rupture Models. *Bulletin of the Seismological Society of America*, *90*(3),
731 604–615.
- 732 Mazzotti, S., Le Pichon, X., Henry, P., & Miyazaki, S.-I. (2000, June). Full inter-
733 seismic locking of the Nankai and Japan-west Kurile subduction zones: An
734 analysis of uniform elastic strain accumulation in Japan constrained by perma-
735 nent GPS. *Journal of Geophysical Research*, *105*(B6), 13159–13177.
- 736 McCaffrey, R., Qamar, A. I., King, R. W., Wells, R., Khazaradze, G., Williams,
737 C. A., ... Zwick, P. C. (2007, June). Fault locking, block rotation and crustal
738 deformation in the Pacific Northwest. *Geophysical Journal International*,
739 *169*(3), 1315–1340.
- 740 McNeill, L. C., Goldfinger, C., Kulm, L. D., & Yeats, R. S. (2000, August). Tec-
741 tonics of the Neogene Cascadia forearc basin: Investigations of a deformed
742 late Miocene unconformity. *Geological Society of America Bulletin*, *112*(8),
743 1209–1224.
- 744 Meade, B. J. (2010). The signature of an unbalanced earthquake cycle in himalayan
745 topography? *Geology*, *38*(11), 987–990.
- 746 Melnick, D. (2016, March). Rise of the central Andean coast by earthquakes strad-
747 dling the Moho. *Nature Geoscience*, *9*(5), 401–407.

- 748 Menant, A., Angiboust, S., Gerya, T., Lacassin, R., Simoes, M., & Grandin, R.
 749 (2020). Transient stripping of subducting slabs controls periodic forearc
 750 uplift. *Nature Communications*, *11*(1823). doi: <https://doi.org/10.1038/s41467-020-15580-7>
 751
- 752 Metois, M., Socquet, A., & Vigny, C. (2012, March). Interseismic coupling, segmen-
 753 tation and mechanical behavior of the central Chile subduction zone. *Journal*
 754 *of Geophysical Research*, *117*(B3), 40–16.
- 755 Metois, M., Vigny, C., & Socquet, A. (2016, April). Interseismic Coupling, Megath-
 756 rust Earthquakes and Seismic Swarms Along the Chilean Subduction Zone
 757 (38°–18°S). *Pure and Applied Geophysics*, *173*(5), 1431–1449.
- 758 Metois, M., Vigny, C., Socquet, A., Delorme, A., Morvan, S., Ortega, I., & Valderas-
 759 Bermejo, C. M. (2013, November). GPS-derived interseismic coupling on the
 760 subduction and seismic hazards in the Atacama region, Chile. *Geophysical*
 761 *Journal International*, *196*(2), 644–655.
- 762 Miller, M. M., Johnson, D. J., Rubin, C. M., Dragert, H., Wang, K., Qamar, A., &
 763 Goldfinger, C. (2001, April). GPS-determination of along-strike variation in
 764 Cascadia margin kinematics: Implications for relative plate motion, subduction
 765 zone coupling, and permanent deformation. *Tectonics*, *20*(2), 161–176.
- 766 Moreno, M., Li, S., Melnick, D., Bedford, J., Baez, J., Motagh, M., . . . others
 767 (2018). Chilean megathrust earthquake recurrence linked to frictional con-
 768 trast at depth. *Nature Geoscience*, *11*(4), 285–290.
- 769 Mouslopoulou, V., Begg, J., Nicol, A., Oncken, O., & Prior, C. (2015). Formation
 770 of late quaternary paleoshorelines in crete, eastern mediterranean. *Earth and*
 771 *Planetary Science Letters*, *431*, 294 - 307. doi: [https://doi.org/10.1016/j.epsl](https://doi.org/10.1016/j.epsl.2015.09.007)
 772 [.2015.09.007](https://doi.org/10.1016/j.epsl.2015.09.007)
- 773 Mouslopoulou, V., Oncken, O., Hainzl, S., & Nicol, A. (2016). Uplift rate transients
 774 at subduction margins due to earthquake clustering. *Tectonics*, *35*(10), 2370-
 775 2384. doi: [10.1002/2016TC004248](https://doi.org/10.1002/2016TC004248)
- 776 Natawidjaja, D. H., Sieh, K., Galetzka, J., Suwargadi, B. W., Cheng, H., Edwards,
 777 R. L., & Chlieh, M. (2007, February). Interseismic deformation above the
 778 Sunda Megathrust recorded in coral microatolls of the Mentawai islands, West
 779 Sumatra. *Journal of Geophysical Research-Solid Earth and Planets*, *112*(B2),
 780 1897–27.

- 781 Niemeijer, A. R., & Spiers, C. J. (2002, January). Compaction creep of quartz-
 782 muscovite mixtures at 500°C: Preliminary results on the influence of muscovite
 783 on pressure solution. *Geological Society, London, Special Publications*, 200(1),
 784 61–71.
- 785 Nishimura, T. (2014, June). Pre-, Co-, and Post-Seismic Deformation of the 2011
 786 Tohoku-Oki Earthquake and its Implication to a Paradox in Short-Term and
 787 Long-Term Deformation. *Journal of Disaster Research*, 9(3), 294–302.
- 788 Nishimura, T., Hirasawa, T., Miyazaki, S., Sagiya, T., Tada, T., Miura, S., &
 789 Tanaka, K. (2004, May). Temporal change of interplate coupling in north-
 790 eastern Japan during 1995–2002 estimated from continuous GPS observations.
 791 *Geophysical Journal International*, 157(2), 901–916.
- 792 Nocquet, J.-M., Villegas-Lanza, J. C., Chlieh, M., Mothes, P. A., Rolandone, F.,
 793 Jarrin, P., ... Yepes, H. (2014, March). Motion of continental slivers and
 794 creeping subduction in the northern Andes. *Nature Geoscience*, 7(4), 287–
 795 291.
- 796 Noda, A. (2016, April). Forearc basins: Types, geometries, and relationships to sub-
 797 duction zone dynamics. *Geological Society of America Bulletin*, 128(5-6), 879–
 798 895.
- 799 Obara, K. (2002). Nonvolcanic deep tremor associated with subduction in southwest
 800 Japan. *Science*, 296(5573), 1679–1681.
- 801 Okada, Y. (1992, April). Internal deformation due to shear and tensile faults in a
 802 half-space. *Bulletin of the Seismological Society of America*, 82(2), 1018–1040.
- 803 Ott, R. F., Gallen, S. F., Wegmann, K. W., Biswas, R. H., Herman, F., & Willett,
 804 S. D. (2019). Pleistocene terrace formation, quaternary rock uplift rates and
 805 geodynamics of the hellenic subduction zone revealed from dating of pale-
 806 oshorelines on crete, greece. *Earth and Planetary Science Letters*, 525, 115757.
 807 doi: <https://doi.org/10.1016/j.epsl.2019.115757>
- 808 Park, J.-O., Tsuru, T., Kodaira, S., Cummins, P. R., & Kaneda, Y. (2002, Au-
 809 gust). Splay Fault Branching Along the Nankai Subduction Zone. *Science*,
 810 297(5584), 1157–1160.
- 811 Paterson, M. S., & Wong, T.-f. (2005). *Experimental Rock Deformation - The Brittle*
 812 *Field*. Springer Science & Business Media.
- 813 Penserini, B. D., Roering, J. J., & Streig, A. (2017, April). A morphologic proxy

- 814 for debris flow erosion with application to the earthquake deformation cycle,
815 Cascadia Subduction Zone, USA. *Geomorphology*, 282(C), 150–161.
- 816 Personius, S. F. (1995). Late Quaternary stream incision and uplift in the forearc
817 of the Cascadia subduction zone, western Oregon - Personius - 1995 - Jour-
818 nal of Geophysical Research: Solid Earth - Wiley Online Library. *Journal of*
819 *Geophysical Research*.
- 820 Philibosian, B., Sieh, K., Avouac, J.-P., Natawidjaja, D. H., Chiang, H.-W., Wu,
821 C.-C., . . . Suwargadi, B. W. (2014, September). Rupture and variable coupling
822 behavior of the Mentawai segment of the Sunda megathrust during the super-
823 cycle culmination of 1797 to 1833. *Journal of Geophysical Research*, 119(9),
824 7258–7287.
- 825 Radiguet, M., Cotton, F., Vergnolle, M., Campillo, M., Walpersdorf, A., Cotte, N.,
826 & Kostoglodov, V. (2012, April). Slow slip events and strain accumulation
827 in the Guerrero gap, Mexico. *Journal of Geophysical Research*, 117(B4),
828 n/a–n/a.
- 829 Rosenau, M., Lohrmann, J., & Oncken, O. (2009, January). Shocks in a box: An
830 analogue model of subduction earthquake cycles with application to seismotec-
831 tonic forearc evolution. *Journal of Geophysical Research*, 114(B1), 183–20.
- 832 Rousset, B., Lasserre, C., Cubas, N., Graham, S., Radiguet, M., DeMets, C., . . .
833 Walpersdorf, A. (2016). Lateral Variations of Interplate Coupling along the
834 Mexican Subduction Interface: Relationships with Long-Term Morphology and
835 Fault Zone Mechanical Properties. *Pure and Applied Geophysics*, 173(10),
836 3467–3486.
- 837 Ruff, L. J., & Tichelaar, B. W. (1996). What Controls the Seismogenic Plate In-
838 terface in Subduction Zones? In *Geophysical monograph series* (pp. 105–111).
839 American Geophysical Union.
- 840 Ryan, W. B. F., Carbotte, S. M., Coplan, J. O., O’Hara, S., Melkonian, A., Arko,
841 R., . . . Zemsky, R. (2009, March). Global Multi-Resolution Topography
842 synthesis. *Geochemistry Geophysics Geosystems*, 10(3), n/a–n/a.
- 843 Sagiya, T. (1999). Interplate coupling in the Tokai District, central Japan, deduced
844 from continuous GPS data. *Geophysical Research Letters*, 26(15), 2315–2318.
- 845 Saillard, M., Audin, L., Rousset, B., Avouac, J.-P., Chlieh, M., Hall, S. R., . . . Far-
846 ber, D. L. (2017, February). From the seismic cycle to long-term deformation:

- 847 linking seismic coupling and Quaternary coastal geomorphology along the
 848 Andean megathrust. *Tectonics*, *36*(2), 241–256.
- 849 Savage, J. C. (1983). A Dislocation Model of Strain Accumulation and Release at
 850 a Subduction Zone. *Journal of Geophysical Research-Solid Earth and Planets*,
 851 *88*(NB6), 4984–4996.
- 852 Savage, J. C., & Thatcher, W. (1992). Interseismic Deformation at the Nankai
 853 Trough, Japan, Subduction Zone. *Journal of Geophysical Research-Solid Earth
 854 and Planets*, *97*(B7), 11117–11135.
- 855 Sawai, Y., Satake, K., Kamataki, T., Nasu, H., Shishikura, M., Atwater, B. F., ...
 856 Yamaguchi, M. (2004). Transient uplift after a 17th-century earthquake along
 857 the Kuril subduction zone. *Science*, *306*(5703), 1918–1920.
- 858 Schmalzle, G. M., McCaffrey, R., & Creager, K. C. (2014, April). Central Casca-
 859 dia subduction zone creep. *Geochemistry Geophysics Geosystems*, *15*(4), 1515–
 860 1532.
- 861 Schurr, B., Asch, G., Rosenau, M., Wang, R., Oncken, O., Barrientos, S., ...
 862 Vilotte, J.-P. (2012). The 2007 m7.7 tocopilla northern chile earthquake
 863 sequence: Implications for along-strike and downdip rupture segmentation and
 864 megathrust frictional behavior. *Journal of Geophysical Research: Solid Earth*,
 865 *117*(B5). doi: 10.1029/2011JB009030
- 866 Seely, D. R., & Dickinson, W. R. (1977). Structure and stratigraphy of forearc re-
 867 gions. *AAPG Special Volumes*, *A122*, 1–23.
- 868 Sieh, K., Natawidjaja, D. H., Meltzner, A. J., Shen, C. C., Cheng, H., Li, K. S., ...
 869 Edwards, R. L. (2008, December). Earthquake Supercycles Inferred from Sea-
 870 Level Changes Recorded in the Corals of West Sumatra. *Science*, *322*(5908),
 871 1674–1678.
- 872 Simoes, M., Avouac, J.-P., Cattin, R., & Henry, P. (2004). The Sumatra subduction
 873 zone: A case for a locked fault zone extending into the mantle. *Journal of Geo-
 874 physical Research: Planets*, *109*(B10).
- 875 Simons, M., Minson, S. E., Sladen, A., Ortega, F., Jiang, J., Owen, S. E., ... Webb,
 876 F. H. (2011, June). The 2011 Magnitude 9.0 Tohoku-Oki Earthquake: Mo-
 877 saicking the Megathrust from Seconds to Centuries. *Science*, *332*(6036),
 878 1421–1425.
- 879 Simpson, G. (2015). Accumulation of permanent deformation during earthquake cy-

- 880 cles on reverse faults. *Journal of Geophysical Research*, *120*, 1958–1974.
- 881 Snyder, N. P., Whipple, K. X., Tucker, G. E., & Merritts, D. J. (2002, June). In-
882 teractions between onshore bedrock-channel incision and nearshore wave-base
883 erosion forced by eustasy and tectonics. *Basin Research*, *14*(2), 105–127.
- 884 Song, T.-R. A., & Simons, M. (2003, August). Large Trench-Parallel Gravity Vari-
885 ations Predict Seismogenic Behavior in Subduction Zones. *Science*, *301*(5633),
886 630–633.
- 887 Spratt, R. M., & Lisiecki, L. E. (2016). A Late Pleistocene sea level stack. *Climate*
888 *of the Past*, *12*(4), 1079–1092.
- 889 Stevens, V. L., & Avouac, J.-P. (2015). Interseismic coupling on the main Himalayan
890 thrust. *Geophysical Research Letters*, *42*(14), 5828–5837.
- 891 Sugiyama, Y. (1994). Neotectonics of Southwest Japan due to the right-oblique sub-
892 duction of the Philippine Sea plate. *Geofísica Internacional*, *33*(1), 53–76.
- 893 Sun, T., Wang, K., & He, J. (2018, June). Crustal Deformation Following Great
894 Subduction Earthquakes Controlled by Earthquake Size and Mantle Rheology.
895 *Journal of Geophysical Research*, *123*(6), 5323–5345.
- 896 Sykes, L. R., Kisslinger, J. B., House, L., Davies, J. N., & Jacob, K. H. (1981). Rup-
897 ture Zones and Repeat Times of Great Earthquakes Along the Alaska-Aleutian
898 ARC, 1784–1980. In D. W. Simpson & P. G. Richards (Eds.), *Earthquake*
899 *prediction an international review* (pp. 73–80). Washington, D. C.: American
900 Geophysical Union.
- 901 Thatcher, W. (1984). The Earthquake Deformation Cycle at the Nankai Trough,
902 Southwest Japan. *Journal of Geophysical Research-Solid Earth and Planets*,
903 *89*(NB5), 3087–3101.
- 904 Trubienko, O., Fleitout, L., Garaud, J.-D., & Vigny, C. (2013, March). Interpreta-
905 tion of interseismic deformations and the seismic cycle associated with large
906 subduction earthquakes. *Tectonophysics*, *589*(C), 126–141.
- 907 Valensise, G., & Ward, S. N. (1991, October). Long-Term Uplift of the Santa-Cruz
908 Coastline in Response to Repeated Earthquakes Along the San-Andreas Fault.
909 *Bulletin of the Seismological Society of America*, *81*(5), 1694–1704.
- 910 van Dinther, Y., Gerya, T. V., Dalguer, L. A., Mai, P. M., Morra, G., & Giardini,
911 D. (2013, December). The seismic cycle at subduction thrusts: Insights from
912 seismo-thermo-mechanical models. *Journal of Geophysical Research*, *118*(12),

- 913 6183–6202.
- 914 Vannucchi, P., Morgan, J. P., Silver, E. A., & Kluesner, J. W. (2016, June). Origin
915 and dynamics of depositional subduction margins. *Geochemistry Geophysics*
916 *Geosystems*, *17*(6), 1966–1974.
- 917 Vergne, J., Cattin, R., & Avouac, J.-P. (2001, September). On the use of disloca-
918 tions to model interseismic strain and stress build-up at intracontinental thrust
919 faults. *Geophysical Journal International*, *147*(1), 155–162.
- 920 von Huene, R., & Lallemand, S. (1990). Tectonic erosion along the Japan and Peru
921 convergent margins. *Geological Society of America Bulletin*, *102*(6), 704–720.
- 922 Wallace, L. M., Beavan, J., McCaffrey, R., & Darby, D. (2004). Subduction zone
923 coupling and tectonic block rotations in the North Island, New Zealand. *Jour-
924 nal of Geophysical Research-Solid Earth and Planets*, *109*(B12), 477–21.
- 925 Wang, K., & Dixon, T. (2004). Coupling semantics and science in earthquake re-
926 search. *Eos, Transactions American Geophysical Union*, *85*(18), 180–180. doi:
927 10.1029/2004EO180005
- 928 Wang, K., & Hu, Y. (2006, June). Accretionary prisms in subduction earthquake cy-
929 cles: The theory of dynamic Coulomb wedge. *Journal of Geophysical Research*,
930 *111*(B6), n/a–n/a.
- 931 Wang, K., & Tréhu, A. M. (2016, August). Invited review paper: Some outstanding
932 issues in the study of great megathrust earthquakes—The Cascadia example.
933 *Journal of Geodynamics*, *98*, 1–18.
- 934 Wang, K., Wells, R., Mazzotti, S., Hyndman, R. D., & Sagiya, T. (2003, January).
935 A revised dislocation model of interseismic deformation of the Cascadia sub-
936 duction zone. *Journal of Geophysical Research*, *108*(B1), 1085–13.
- 937 Wells, R. E., Blakely, R. J., Sugiyama, Y., Scholl, D. W., & Dinterman, P. A.
938 (2003). Basin-centered asperities in great subduction zone earthquakes: A
939 link between slip, subsidence, and subduction erosion? *Journal of Geophysical*
940 *Research: Planets*, *108*(B10).
- 941 Willett, S. D., Beaumont, C., & Fullsack, P. (1993). Mechanical Model for the Tec-
942 tonics of Doubly Vergent Compressional Orogens. *Geology*, *21*(4), 371–374.
- 943 Ye, L., Lay, T., & Kanamori, H. (2013, November). Large earthquake rupture pro-
944 cess variations on the Middle America megathrust. *Earth and Planetary Sci-
945 ence Letters*, *381*(C), 147–155.

- 946 Yoshikawa, T. (1968, December). Seismic Crustal Deformation and its Relation to
947 Quaternary Tectonic Movement on the Pacific Coast of Southwest Japan. *The*
948 *Quaternary Research (Daiyonki-Kenkyu)*, 7(4), 157–170.
- 949 Yoshikawa, T., Kaizuka, S., & Ôta, Y. (1981). *The landforms of Japan* /. Tokyo:
950 University of Tokyo Press.
- 951 Yoshioka, S., Yabuki, T., Sagiya, T., Tada, T., & Matsu'ura, M. (1993). Interplate
952 coupling and relative plate motion in the Tokai district, central Japan, deduced
953 from geodetic data inversion using ABIC. *Geophysical Journal International*,
954 113, 607–621.
- 955 Yue, H., Lay, T., Rivera, L., An, C., Vigny, C., Tong, X., & Báez Soto, J. C. (2014,
956 October). Localized fault slip to the trench in the 2010 Maule, Chile $M_w = 8.8$
957 earthquake from joint inversion of high-rate GPS, teleseismic body waves,
958 InSAR, campaign GPS, and tsunami observations. *Journal of Geophysical*
959 *Research*, 119(10), 7786–7804.